


## RESEARCH ARTICLE

## OPEN ACCESS

# Differential Diagnosis of Brain Tumors Using Principal Component Analysis to Identify Highly Correlated PWI, DWI, and MRS Parameters Relevant to Tumor Type Identification



Camilla Russo<sup>1,\*</sup> , Adriana Cristofano<sup>1</sup>, Fabrizia Cavaliere<sup>2</sup>, Simone Coluccino<sup>3</sup>, Pasqualino De Marinis<sup>4</sup>, Alessandra Alfieri<sup>4</sup>, Giovanna Mazzarella<sup>5</sup>, Ferdinando Caranci<sup>6</sup> and Eugenio Maria Covelli<sup>1,7</sup>

<sup>1</sup>Department of Neurosciences, "Santobono-Pausilipon" Children's Hospital, Naples, Italy

<sup>2</sup>Department of Advanced Biomedical Sciences, University of Naples "Federico II", Naples, Italy

<sup>3</sup>Neuroradiology Unit, Head-Neck Department, "San Giuseppe Moscati" Hospital, Avellino, Italy

<sup>4</sup>Neurosurgical Unit, "Sant'Anna e San Sebastiano" Hospital, Caserta, Italy

<sup>5</sup>Pathology Unit, "Sant'Anna e San Sebastiano" Hospital, Caserta, Italy

<sup>6</sup>Precision Medicine Department, University of Campania Luigi Vanvitelli, Naples, Italy

<sup>7</sup>Neuroradiology Unit, "Sant'Anna e San Sebastiano" Hospital, Caserta, Italy

## Abstract:

**Introduction:** Differentiating brain tumors through neuroimaging is challenging due to overlapping radiological features, requiring advanced techniques and clinical correlation for accurate diagnosis. The aim of this retrospective observational monocentric study is to determine the diagnostic performance of combining perfusion-weighted imaging (PWI), diffusion-weighted imaging (DWI), and magnetic resonance spectroscopy (MRS) for MRI-based differential diagnosis of the three major classes of adult malignant intra-axial brain tumors. Principal component analysis (PCA) is applied to identify relevant imaging features, with the goal of supporting preoperative diagnosis beyond conventional MRI alone.

**Methods:** We selected 72 adult patients who underwent MRI examination, including DWI, PWI, and MRS imaging before surgery, for suspected malignant intra-axial expansive lesions (namely glioblastoma, metastasis, or primary non-Hodgkin lymphoma). The definitive histological diagnosis was obtained on post-operative specimens. Quantitative variables derived from DWI, PWI, and MRS acquisition were identified and processed using principal component analysis. The differences between groups for the most relevant parameters identified by PCA were then tested by the Kruskal-Wallis test.

**Results:** Finally, a total of 11 specimens of non-Hodgkin lymphomas, 18 specimens of single metastases, and 43 specimens of wild-type glioblastomas were gathered. CBF, CBV, MTT, ADC, and lipid-lactate (Lip-Lac) at MRS were found to be the most relevant variables for differential diagnostic purposes through PCA analysis. In particular, ADC and Lip-Lac were more strongly associated with differentiating lymphoma from the other two disease classes, while CBF, CBV, and MTT contributed more to differentiating glioblastoma from metastasis.

**Discussion:** In this study, ADC and Lip-Lac differentiated CNS lymphoma, while CBV, CBF, and MTT distinguished GBM from metastases, supporting PCA's clinical value beyond diagnostic workflows.

**Conclusion:** The combined use of PWI, DWI, and MRS can assist the radiologist in accurate preoperative differential diagnosis of the three main classes of adult malignant intra-axial brain neoplasms, enhancing diagnostic performance beyond that of conventional MRI alone.

**Keywords:** Magnetic resonance imaging, Oncology, Glioma, Lymphoma, Metastasis, Principal component analysis.

© 2025 The Author(s). Published by Bentham Open.

This is an open access article distributed under the terms of the Creative Commons Attribution 4.0 International Public License (CC-BY 4.0), a copy of which is available at: <https://creativecommons.org/licenses/by/4.0/legalcode>. This license permits unrestricted use, distribution, and reproduction in any medium, provided the original author and source are credited.



Received: March 27, 2025

Revised: June 22, 2025

Accepted: July 01, 2025

Published: September 24, 2025



Send Orders for Reprints to  
[reprints@benthamscience.net](mailto:reprints@benthamscience.net)

\*Address correspondence to this author at the Neuroradiology Unit, Department of Neurosciences, "Santobono-Pausilipon" Children's Hospital, Via Mario Fiore 6, 80129, Naples, Italy; Tel: 0039 081 2205682; E-mail: [camilla\\_russo@hotmail.it](mailto:camilla_russo@hotmail.it)

Cite as: Russo C, Cristofano A, Cavaliere F, Coluccino S, De Marinis P, Alfieri A, Mazzarella G, Caranci F, Covelli E. Differential Diagnosis of Brain Tumors Using Principal Component Analysis to Identify Highly Correlated PWI, DWI, and MRS Parameters Relevant to Tumor Type Identification. *Open Neuroimaging J*, 2025; 18: e18744400398879. <http://dx.doi.org/10.2174/0118744400398879250922161854>

## 1. INTRODUCTION

The actual global age-standardized incidence of primary malignant brain tumors is about 3.5 per 100,000 per year for males and 2.6 per 100,000 per year for females. These rates are higher in Western countries, probably due to differences in life expectancy and access to advanced diagnostic technologies compared to less developed countries. The most common types of malignant brain tumors vary significantly by age group, with high-grade gliomas, brain metastases, and central nervous system (CNS) lymphomas being the most frequent histological types in adults. Although CNS tumors are relatively rare in adults, they are a significant cause of reduced life quality, functional limitation of daily activities, and life shortening [1-3].

Continuous advancements in diagnostic technologies and imaging tools are progressively improving the identification of brain tumors. Magnetic resonance imaging (MRI) remains the most important technique for this purpose, offering an optimal balance between tissue characterization and anatomical details, thus playing a crucial role from the initial clinical evaluation to the monitoring of tumor recurrence in patients diagnosed with brain tumors [4, 5]. Due to MRI, radiologists are now responsible for providing not only morphological data on tumor structure but also functional information, such as tumor vascularization, metabolite concentrations, cellular density, and white matter fiber integrity. This detailed characterization of pathological tissue often enables preliminary tumor type classification even before surgical intervention and histopathological examination, thereby contributing to early diagnosis and improved patient management [5]. However, modern radiologists must address the challenge of managing the increasing volume and complexity of data generated by a single MRI examination, and of integrating this information to support the most accurate and comprehensive diagnosis possible.

The same considerations apply to MRI data used for computational analysis on large datasets. As the number of extracted features increases, the volume of data required to achieve statistically significant results also grows. This can lead to reduced diagnostic accuracy due to dimensionality problems, specifically when multiple and multiparametric MRI sequences are used, as the number of possible combinations of imaging features becomes extremely large. Evaluating and simplifying the complexity

in imaging data is particularly critical in the context of AI-based technologies applied to cancer detection [6, 7]. To address this problem, preliminary feature selection can be employed to reduce dimensionality while preserving as much imaging information as possible. Among dimensionality reduction procedures, one of the most adopted techniques is principal component analysis (PCA) [8], generally used in machine learning and artificial neural networks [9, 10], but potentially applicable also to other frameworks [11, 12].

We hypothesized that using a PCA-based statistical approach could help reduce data redundancy and assist radiologists in prioritizing MRI features with the greatest diagnostic value for distinguishing among the three main types of adult malignant intra-axial brain tumors. Building on this premise, the goal of the study is to evaluate the diagnostic performance of combining diffusion-weighted imaging (DWI), perfusion-weighted imaging (PWI), and magnetic resonance spectroscopy (MRS) for MRI-based differential diagnosis. PCA is applied to identify which parameters from these sequences are most informative in this specific clinical context. Ultimately, this approach may contribute to more efficient imaging protocols and support clinical decision-making by enhancing the interpretation of multiparametric MRI in a statistically robust manner.

## 2. MATERIALS AND METHODS

In this retrospective, observational, monocentric study, we analyzed MRI data of patients referred to the emergency department of "Sant'Anna e San Sebastiano" Hospital, Caserta, for headache or focal neurological symptoms between 2018 and 2020, who underwent brain computed tomography and were found to have a positive result for a suspected malignant brain expansive lesion. These patients subsequently underwent brain MRI examination for pre-surgical lesion identification and characterization, including DWI, PWI, and MRS sequences. Patients who refused MRI and those whose MRI was affected by motion or device-related artifacts were excluded from the analysis. The same exclusion criteria applied to patients who refused surgery or brain biopsy, patients with tumefactive lesions other than brain tumors, and patients with no or inconclusive pathological examination results. Other exclusion criteria were previous brain surgery or panencephalic radiotherapy. All patients underwent a standard contrast-enhanced MRI examination on the same 1.5T scan unit (Philips Ingenia, Philips, Best,

The Netherlands) using the same 16-channel head coil. Concerning the three above-mentioned sequences, the acquisition parameters were set as follows:

- Spin-echo echo-planar axial DWI sequence, including two b-values ( $b=0$ ,  $b=1000 \text{ s/mm}^2$ ), with corresponding apparent diffusion coefficient (ADC) map reconstruction;
- Echo planar axial dynamic susceptibility contrast (DSC) MR PWI during a 5 ml gadolinium-based contrast media bolus at a rate of 5 ml/sec, followed by a 20 ml saline flush. According to recent recommendations, DSC acquisition was preceded by 5 ml gadolinium-based contrast media and 20 ml saline flush administration to pre-saturate brain tissue and reduce T1 contamination in DSC imaging. Manual region of interest (ROI) placement was performed by two neuroradiologists in consensus on the solid enhancing portion of the tumor on post-contrast 3D T1w images, and such defined ROI was then transferred on color maps (*i.e.* cerebral blood flow (CBF), cerebral blood volume (CBV), mean transit time (MTT), and time to peak (TTP) maps); relative values were then computed on the local workstation by an experienced neuroradiologist;
- MRS with single-voxel technique (intermediate TE=144ms, TR=3sec, TM=14ms), with  $1.5 \times 1.5 \times 1.5$  voxel and slice-selection gradient strength of 0.15G/cm; voxel was positioned on volumetric pre-contrast images (both T2w and T1w, depending on the single case). Metabolite spectra with corresponding ratios were computed on the local workstation by an experienced neuroradiologist.

Histological diagnosis was obtained on post-operative specimens by an experienced neuropathologist, who finally identified 11 cases of non-Hodgkin lymphoma (NHL), 18 cases of single brain metastasis (MET), and 43 cases of wild-type glioblastoma (GBM).

MRI DICOM data from each examination were anonymized and locally stored. Quantitative variables derived from DWI, PWI, and MRS acquisitions encompassed: ADC values from the DWI sequence; CBV, CBF, MTT, and TTP values within the specific ROI from the DSC PWI acquisition; metabolite peaks, such as lipid-lactates (Lip-Lac), N-acetylaspartate (NAA), choline (Cho), and creatine (Cr), with their ratios from MRS acquisition. To minimize information loss, the above-mentioned quantitative variables derived from DWI, PWI, and MRS acquisitions were analyzed and plotted using CA [13]. PCA was performed for dimensionality reduction and exploratory data analysis, as it transforms a set of possibly correlated

variables into a smaller set of uncorrelated variables called principal components (PCs). These components are linear combinations of the original variables and are ordered so that the first component captures the maximum possible variance in the data, the second captures the maximum remaining variance orthogonal to the first, and so on. Before PCA, variables were standardized by calculating their means and standard deviations, and then applying the standardization formula  $z = (x - \mu) / \sigma$ . To determine how many PC to retain, a scree plot graph was obtained. To determine whether the differences among the three groups (NHL, GBM, and MET) were significant, the Kruskal-Wallis test was used. Finally, for relevant parameters, between-groups differences (NHL vs. GBM, GBM vs. MET, and MET vs. NHL) were tested using the Wilcoxon signed-rank test. An original  $p$ -value of less than 0.01 was set, followed by Bonferroni correction to adjust for multiple comparisons. For all analyses, a final significance level of  $p = 0.0011$  (Bonferroni-corrected) was established. Statistical analyses were performed using the XLStat package v.2019. An example of an MRI of the three malignant brain lesions included in the analysis is shown in Fig. (1). Demographic data and the prevalence of final histological diagnoses in our sample are summarized in Table 1.

### 3. RESULTS

We collected homogeneous and complete MRI data of 72 adult patients (M:F 45:27; mean age $\pm$ SD 59.6 $\pm$ 12.4). At histological examination, lesions were classified into 11 NHL, 18 MET, and 43 wild-type GBM; concerning single brain metastases, 9 originated from lung cancer (8 adenocarcinoma and 1 microcitoma), 4 from breast cancer, 2 from upper digestive system neoplasm, 2 from bladder cancer, and 1 from skin melanoma. Despite the different pathological origins, due to the relatively limited sample size, metastases were analyzed as a single group. The unbalanced distribution of the sample in this study reflects the actual prevalence of the disease subtypes in the general population [2, 3]. Rather than artificially balancing the groups, which could introduce bias or reduce ecological validity, we opted to preserve the natural proportions to enhance the clinical applicability of the findings; this approach ensures that the proposed model remains grounded in real-world conditions, thereby improving generalizability and relevance to everyday diagnostic and treatment decisions. No statistical difference concerning demographics was observed in the three subgroups.

**Table 1. Patients' data summary. Patients' demographical data and pathological diagnoses prevalence.**

-	Patients (n)	Prevalence (%)	M:F	Age $\pm$ SD
<b>Total</b>	72	100%	45:27	59.6 $\pm$ 12.4
<b>Wild-Type Glioblastoma</b>	43	59.7%	28:15	62 $\pm$ 15.5
<b>Non-Hodgkin Lymphoma</b>	11	15.3%	6:5	58.4 $\pm$ 11.8
<b>Single Brain Metastasis</b>	18	25%	11:7	61.3 $\pm$ 12.6

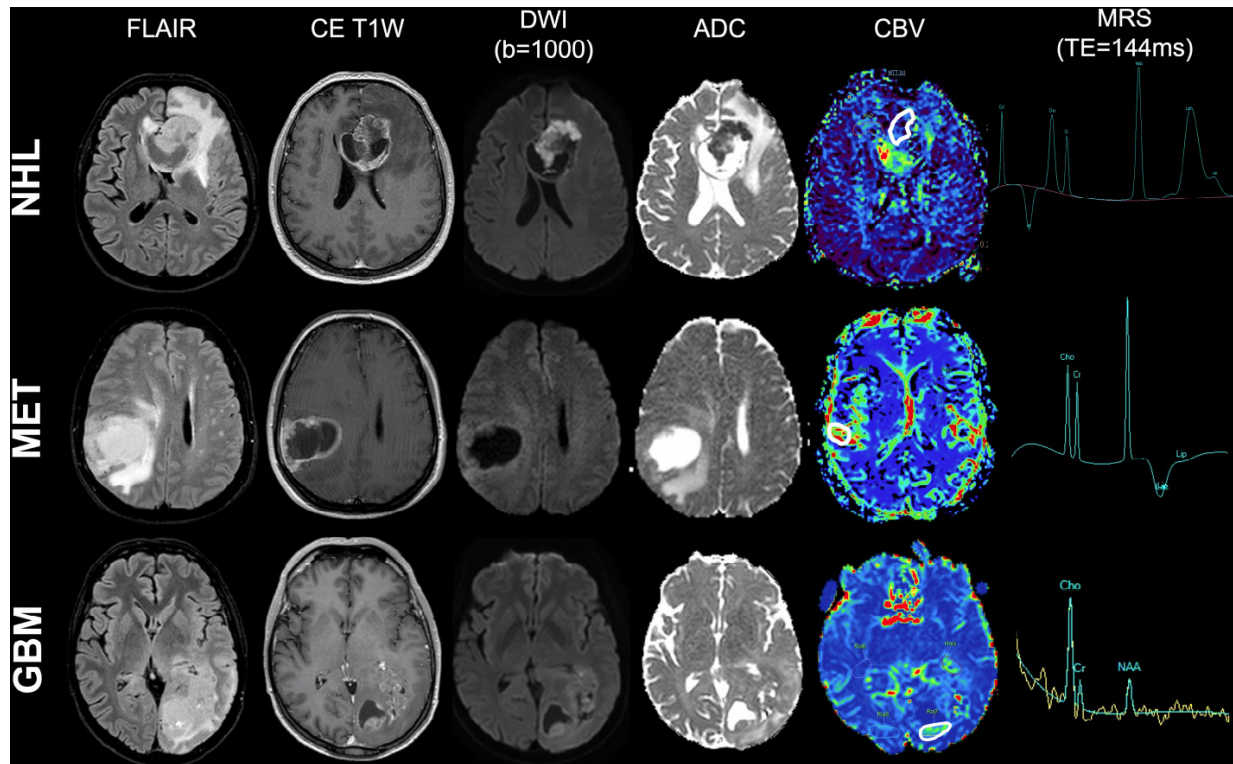


**Fig. (1). Example of conventional MRI findings in the three most common adult brain tumor types.** Three examples of conventional MRI findings in non-Hodgkin lymphoma (first row), single brain metastasis (second row), and wild-type glioblastoma (third row): **A**) FLAIR imaging; **B**) post-contrast T1w imaging; **C**) b-1000 DWI and **D**) relative ADC map; **E**) CBV map from DSC-PWI, with ROI placement (white continuous line); **F**) MRS metabolite spectrum (TE=144 ms).

To define which were the most informative parameters among the ones obtained in DWI, PWI, and MRS, the statistical procedure of PCA was used to summarize the information content of these variables and identify among them a smaller set of informative indices that could be more easily visualized and analyzed. PC-1 captures the maximum possible variance in the data (29.1%), and PC-2 captures the maximum remaining variance orthogonal to the first (18.8%). The scree plots graph showed the eigenvalues ( $\lambda$ ) in ascending order ( $\lambda$  indicate how much of the total variance in the data is captured by each PC; higher  $\lambda$  means that the corresponding PC accounts for a greater portion of the variability in the dataset); the point where the curve starts to flatten (PC<sub>5</sub>) indicates the optimal number of components considered. A summary of PCA results is shown in Fig. (2), while the scree plot graph is shown in Fig. (3);  $\lambda$ , variance, and cumulative variance of PC parameters deriving from PCA are listed in Table 2. By interpreting each PC and examining the magnitude and direction of the coefficients, it was found that PC-1 has a large association with DWI-derived ADC values, as well as with CBF and CBV PWI-derived parameters, while PC-2 has a large association with MTT from PWI and Lip-Lac ratio from MRS. Kruskal-Wallis test was used to confirm

such evidence and compute  $p$ -values, confirming significant results for ADC ( $p=2.7e-06$ ), Lip-Lac ( $p=4.4e-07$ ), CBV ( $p=2.5e-08$ ), CBF ( $p=1e-10$ ), and MTT ( $p=5.6e-05$ ). Therefore, the identified parameters were considered for further analysis. Indeed, when comparing the impact of each MRI-derived metric identified at PCA in the three groups (NHL, GBM, and MET) by means of the Wilcoxon signed-rank test (Bonferroni corrected), we obtained significant results for:

- ADC in differentiating NHL and the other two groups of lesions ( $p=9.6e-07$  for GBM and  $p=3.4e-05$  for MET, respectively);
- Lip-Lac in differentiating NHL from the other two groups of lesions ( $p=1.1e-06$  for GBM and  $p=2.4e-07$  for MET, respectively);
- CBF in differentiating GBM from the other two groups of lesions ( $p=6.8e-11$  for NHL and  $p=4.4e-10$  for MET, respectively);
- CBV in differentiating GBM from the other two groups of lesions ( $p=6.8e-11$  for NHL and  $p=2.0e-05$  for MET, respectively);
- MTT in differentiating GBM from the other two groups of lesions ( $p=0.00051$  for NHL and  $p=0.0006$  for ME, respectively).



**Table 2. Eigenvalues, percentage of variance, and cumulative variance of PC parameter deriving from PCA.  $\lambda$  is used as abbreviation for eigenvalue; variance and cumulative variance are expressed as percentages (%).**

-	PC <sub>1</sub>	PC <sub>2</sub>	PC <sub>3</sub>	PC <sub>4</sub>	PC <sub>5</sub>	PC <sub>6</sub>	PC <sub>7</sub>	PC <sub>8</sub>	PC <sub>9</sub>
$\lambda$	26.196	16.883	13.818	11.134	0.7558	0.5596	0.3947	0.2988	0.1879
Variance	291.065	187.593	153.535	123.711	83.978	62.181	4.386	33.195	20.882
Cumulative	291.065	478.658	632.193	755.904	839.882	902.063	945.923	979.118	100

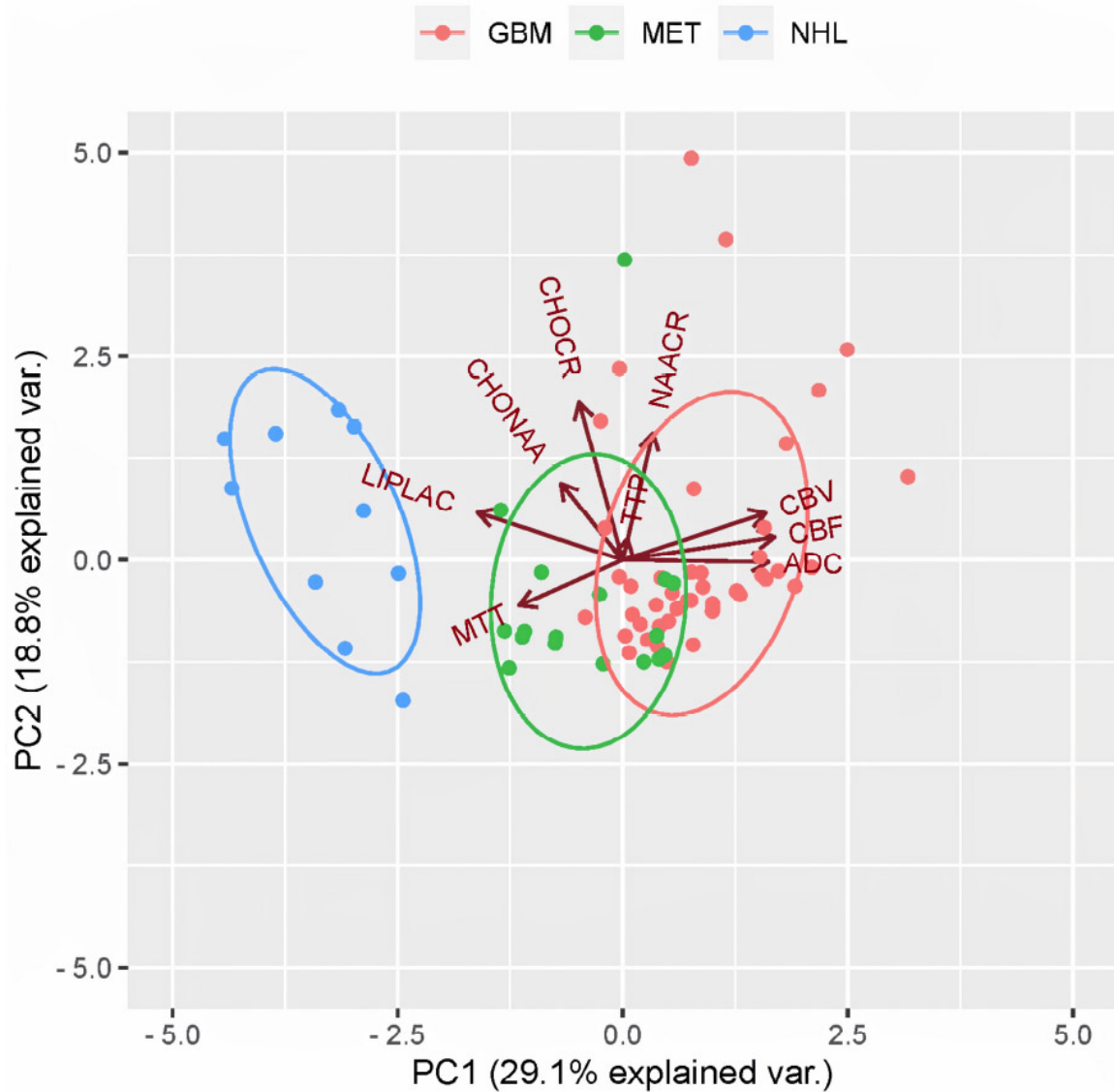


**Fig. (2). PCA factor map.** Factor map of the PCA performed on the 3 different pathological groups (NHL, GBM, and MET, respectively) and the 9 considered MRI-derived quantitative variables (namely: ADC, CBV, CBF, MTT, TTP, Lip-Lac, Cho-NAA, Cho-Cr, and NAA-Cr). Points represent observations (that are close to each other on the map are similar in their underlying variable patterns), with different colors representing the 3 different pathological groups (blue for NHL, red for GBM and green for MET); ellipses represent 68% confidence intervals of core regions; arrows (vectors) show the contribution of each original variable to the components, with arrows' directions representing the correlation between variable-principal component and arrows' length representing the magnitude of the correlation. PC-1 (x-axis) and PC-2 (y-axis) correspond to the first and second principal components, respectively, accounting for the highest and second-highest variance in the dataset. Variables pointing in similar directions are positively correlated, while those pointing in opposite directions are negatively correlated.

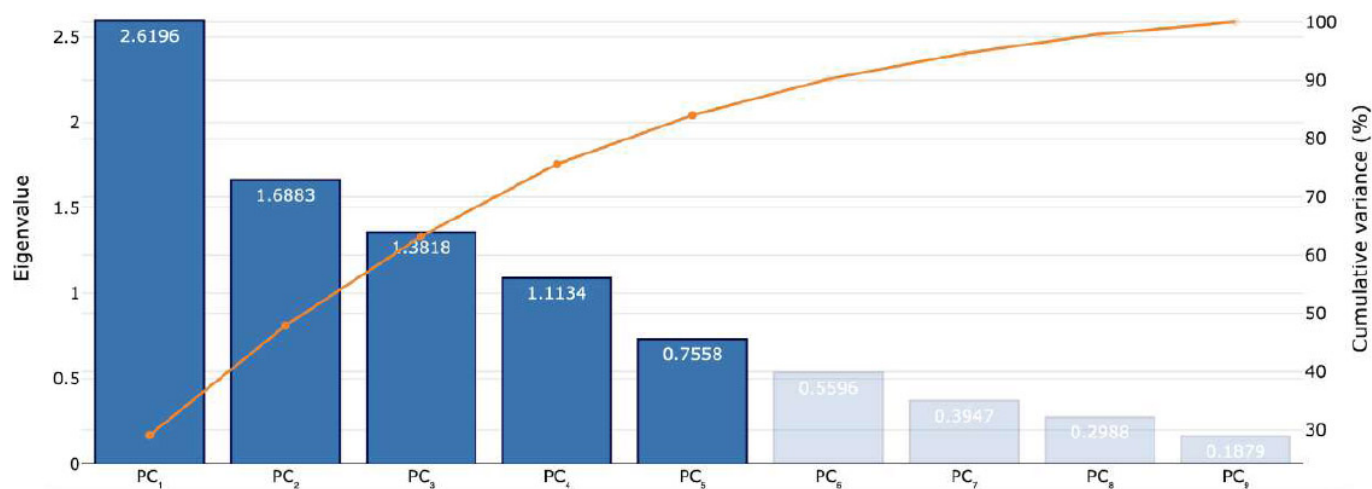


**Fig. (3). Scree plot from PCA analysis.** The scree plot displays the number of the principal component *versus* their corresponding eigenvalue, as well as the cumulative variance (%) explained.

A similar trend was also observed for CBF and CBV in differentiating between MET and NHL ( $p=0.00073$  and  $p=0.0056$ , respectively). No significant result was observed for ADC and Lip-Lac in differentiating between GBM and MET ( $p=0.42$  and  $p=0.022$ , respectively) and for MTT in differentiating between NHL and MET ( $p=0.72$ ).

A summary of Kruskal-Wallis test and Wilcoxon signed-rank test results concerning significant parameters identified at PCA, coupled to boxplot and data dispersion representation, is shown in Fig. (4). Conversely, Kruskal-Wallis results concerning non-significant parameters identified at PCA are reported as Supplementary Material.

#### 4. DISCUSSION

PCA is a reliable statistical technique that can enhance the diagnostic value of MRI by identifying the most relevant imaging parameters in complex clinical datasets. When numerous MRI sequences and quantitative metrics are collected during imaging acquisition, PCA reduces dimensionality while preserving the variance that best represents the underlying data structure and highlights patterns that may not be immediately apparent, thus identifying which MRI parameters contribute most to distinguishing different nosological entities. PCA is commonly adopted in neuroimaging studies in contexts involving large-scale data, such as radiomics or deep learning, where high-dimensional feature sets are extracted from MRI scans [14-17]. For example, in recent times, Akbari *et al.* demonstrated that PCA of DSC MRI could effectively quantify tumor microenvironment acidity in glioblastoma. In contrast, Gaikwad *et al.* reported that combining PCA with a probabilistic neural network enabled accurate classification of brain tumors based on imaging data [10, 18]. By contrast, PCA is less commonly applied to the

more limited sets of quantitative parameters typically derived from conventional MRI sequences in standard neuro-oncological protocols, such as ADC values from DWI, CBV from PWI, or metabolite ratios from MRS; these datasets usually include only a handful of well-characterized variables, making dimensionality reduction seem less urgent. Even in such cases, PCA can reveal latent patterns, reduce variable correlation, and identify key diagnostic parameters, especially when multiple quantitative sequences are combined. Despite its routine use in AI-based workflows, its limited adoption in clinical practice may be a missed opportunity to improve diagnostic accuracy and streamline interpretation.

With this background, we hypothesize that PCA applied to data from DWI, DSC-PWI, and single-voxel MRS MRI images of patients with suspected brain tumors may help to identify the most informative imaging-derived parameters to assist the radiologist in accurately predicting brain tumor type before pathological examination. CBF, CBV, MTT, ADC, and Lip-Lac at MRS were found to be the most relevant MRI-derived indices for differential diagnostic purposes in brain tumor allocation; in particular, ADC and Lip-Lac contributed more to the differentiation of NHL from the other two disease classes, while MTT, CBF, and CBV contributed more to the differentiation of GBM from MET. Some recent studies provided the evidence that DWI, PWI and MRS can be used as reference techniques to diagnose different brain malignancies with a greater level of sensitivity and accuracy, by means of simple descriptive statistics [19]; the major strength of our analysis is given by the confirmatory role of PCA in determining which PWI, DWI, and MRS MRI-derived metrics may be more informative in the specific clinical setting of brain tumor in adult patients.

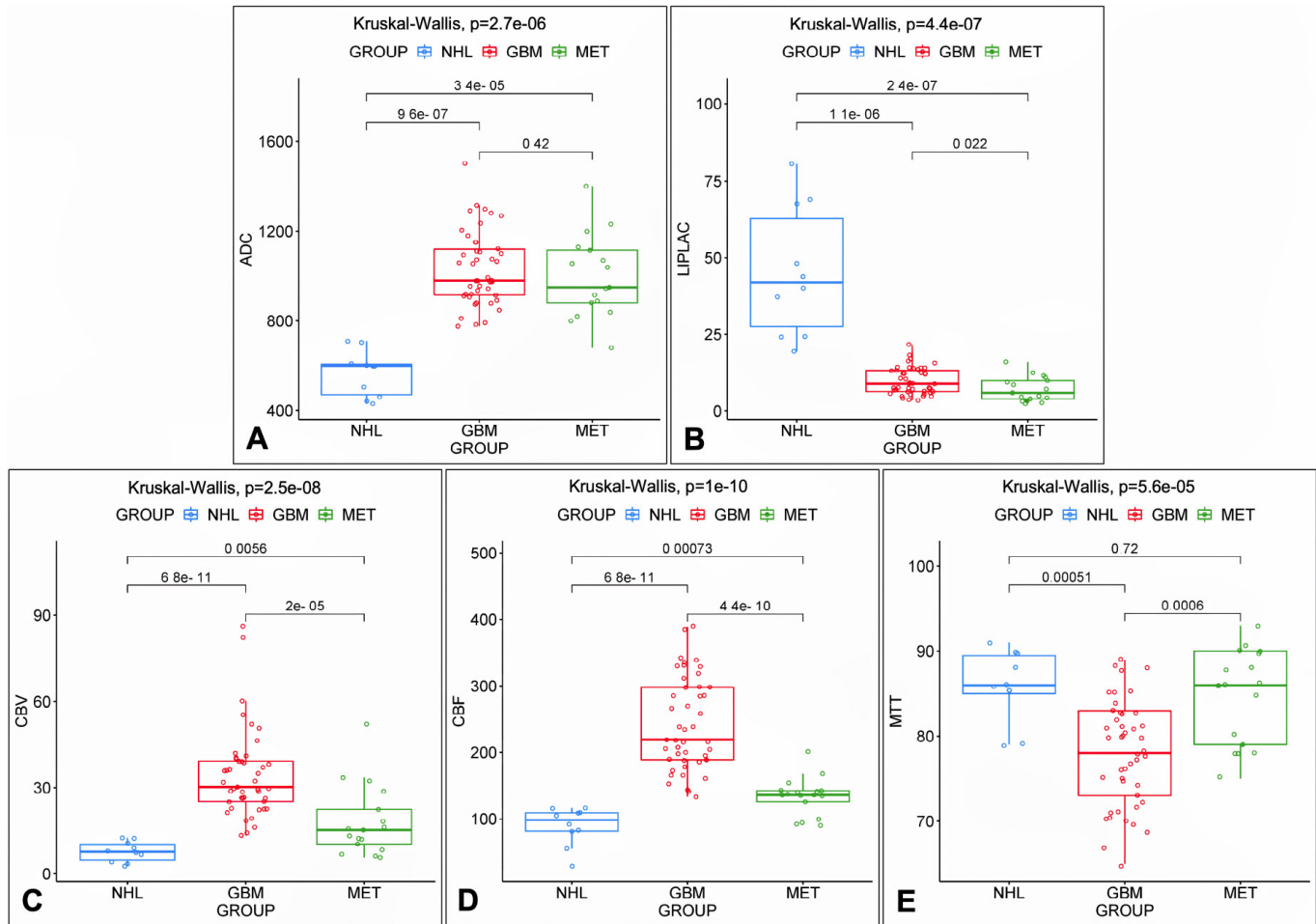


**Fig. (4). Scattered boxplots of the most relevant indices identified at PCA.** Scattered boxplots of the most relevant indices identified at PCA, with data dispersion and minimum value/median value/maximum value/quartiles/inter-quartiles ranges concerning ADC (A), Lip-Lac (B), CBV (C), CBF (D), and MTT (E) in the three pathological groups: NHL (red), wild-type GBM (blue), and single brain MET (green);  $p$ -values among groups (Bonferroni corrected) are also reported on the top of each boxplot table.

The most used diffusion metric at MRI examination is represented by ADC values [20-23], whose correlation with tumor cellularity has been explored in several studies over the years [24-28], although sometimes with some controversial results [29, 30]. Highly cellular tissues, such as aggressive brain lesions, typically show lower ADC values. ADC has been proposed as a standalone tool for tumor differentiation; for example, dysembryoplastic neuroepithelial tumors in children display higher ADC than more common pediatric tumors [31]. However, results are inconsistent when using ADC to distinguish tumor subgroups, such as between GBM subtypes [32] or low-grade astrocytomas and oligodendrogliomas [33]. The most established adult application remains identifying primary CNS lymphoma, which consistently shows lower ADC values than glial or metastatic lesions [23, 26, 33, 34, 35]. Our results, in line with this evidence [35], support the central role of ADC measurements in differential diagnosis of brain tumors, with PCA analysis revealing its major contribution in the identification of CNS lymphomas

(namely, the tumor with the most marked restriction in diffusion coefficients). Conversely, the lack of significance for ADC in differentiating GBM from brain MET provides a further contribution to understanding the role of diffusion in this specific setting, helping to clarify some of the conflicting findings reported in the scientific literature [36, 37].

Angiogenesis is essential for tumor growth and spread; MRI perfusion and vascular microstructure analysis aid in both differential diagnosis and monitoring. Among PWI techniques, including DSC, dynamic contrast enhanced (DCE), and arterial spin labeling (ASL), DSC-PWI is the most studied and widely used in clinical practice [24, 38]. DSC is based on the principle of susceptibility signal loss on T2\*w images during intravenous administration of gadolinium-based contrast agent; signal intensity/time curves are the final output of such progressive signal loss and are translated into color maps, including MTT, CBF, and CBV. DSC-PWI parameters, namely CBF and CBV

maps, were demonstrated to outperform and be interchangeable in assessing tumor vascularity compared to other perfusion parameters, which are generally more discordant [38-42]. In particular, DSC perfusion curves in high-grade glial lesions usually return very quickly close to baseline, whereas perfusion curves in tumors with leaky capillaries, such as metastases, do not have the same trend. Our results confirm this finding, proposing a major role for CBV and CBF parameters in distinguishing highly proliferative lesions like GBM from metastases or CNS lymphoma [43], and a minor supportive role in distinguishing between MET and NHL. Conversely, MTT has been more frequently used as an indirect indicator of deficient microvascular blood flow control in treatment-resistant and recurrent brain tumors. In contrast, its role in distinguishing high-grade brain tumors is less accurately known and ancillary to CBF/CBV changes [43-45]; however, these findings suggest that MTT variations are consistent with CBF and CBF fluctuations, moving in the same direction and providing additional information on tumoral vascularity and hemodynamics.

Finally, MRS reveals the biochemical profile of pathological brain tissues, indicating high cellular turnover, disrupted neuronal homeostasis, and anaerobic metabolism. Proton MRS is most commonly used, with intermediate TE (144 ms) typically allowing identification of key tumor metabolites. While both single- and multi-voxel techniques are available, single voxel MRS is preferred in brain tumors for its diagnostic adequacy and shorter acquisition time [38, 46, 47]. Brain neoplasms typically present with elevated Cho and decreased NAA, as confirmed by several studies where the presence of neoplastic lesions was indicated by an altered Cho/NAA ratio at intermediate/long TE. Conversely, the potential for MRS in distinguishing brain tumor types is more controversial, with the most significant contribution for Lip-Lac peak in CNS lymphoma identification; however, such finding may be superimposable to the one observed in different high-grade brain tumors with evidence of high cell membrane turnover, such as glioblastoma (especially when large necrotic areas are present) [48-50]. In our cohort, in line with this last evidence, Lip-Lac evaluation at intermediate TE was the only contributive MRS parameter, useful in differentiating NHL from the other two groups of brain tumors; no significant result emerged for the other considered metabolite ratios. The same applies to the Lip-Lac peak that fails in distinguishing between GBM and MET, while it is known that MRS may provide a more consistent contribution when performed in peritumoral surrounding edema [51]; however, for this purpose, MRS's role becomes particularly evident when combined with other advanced MRI imaging modalities [52].

## CONCLUSION

PCA statistical approach helps in reducing redundancy and supporting the radiologist in focusing on MRI features with the highest diagnostic impact; ultimately, this method can facilitate the development of optimized imaging

protocols and improve clinical decision-making by refining the interpretation of multiparametric MRI data in a statistically robust manner. By means of PCA analysis, we demonstrated how the combined use of DWI, DSC-PWI, and MRS can assist the radiologist in an accurate pre-operative differential diagnosis of the three main classes of adult malignant intra-axial brain tumors, increasing the diagnostic performance obtained with conventional MRI alone. The most informative parameters deriving from this preliminary study are represented by ADC values, MTT, CBV, CBF, and Lip-Lac peak. These results strongly suggest a potential role for a combined PCA-based approach to multiparametric advanced MRI imaging, even across different technical settings and potentially in various clinical scenarios. However, further studies on larger samples or involving different disease categories are still needed to validate and generalize the presented results; our medium- to long-term objective is to apply the same approach to a larger sample of subjects, including acquisitions obtained using different MRI systems or imaging studies concerning lesions of various types that may be relevant to the differential diagnosis of the most common adult brain tumors.

## LIMITATIONS

This study suffers from some limitations that must be stated and discussed. The first one regards the retrospective monocentric design of the study, which does not allow for further analysis and speculations on the role of advanced MRI techniques in the diagnosis of brain tumors. Secondly, the sample size is somewhat limited, taking into account the incidence of these pathologies in Western countries; however, despite the limited body of collected evidence, the sample has the merit of being very homogeneous, as all patients underwent the same comprehensive MRI examination. As a last consideration, the presented results only apply to a specific clinical setting (*i.e.*, machine vendor, field strength, type of head coil, MRI protocol with specific sequence type and parameters, *etc.*) and can be somehow influenced by observers' experience at the moment of data collection; for this reason, the same approach should be tested in different settings to generalize its performance.

## AUTHORS' CONTRIBUTIONS

It is hereby acknowledged that all authors have accepted responsibility for the manuscript's content and consented to its submission. They have meticulously reviewed all results and unanimously approved the final version of the manuscript.

## LIST OF ABBREVIATIONS

ADC	=	apparent diffusion coefficient
ASL	=	arterial spin labeling
CBF	=	cerebral blood flow
CBV	=	cerebral blood volume
Cho	=	choline



CNS	=	central nervous system
Cr	=	creatine
DCE	=	dynamic contrast enhanced
DSC	=	dynamic susceptibility contrast
DWI	=	diffusion-weighted imaging
GBM	=	glioblastoma
Lip-Lac	=	lipid-lactate
MET	=	metastasis
MRI	=	magnetic resonance imaging
MRS	=	magnetic resonance spectroscopy
MTT	=	mean transit time
NAA	=	N-acetylaspartate
NHL	=	non-Hodgkin lymphoma
PC	=	principal component
PCA	=	principal component analysis
PWI	=	perfusion weighted imaging
ROI	=	region of interest
SD	=	standard deviation
TE	=	echo time
TTP	=	time to peak
$\lambda$	=	eigenvalue

## ETHICS APPROVAL AND CONSENT TO PARTICIPATE

Formal ethical approval was waived for this study, as this is a non-experimental retrospective study, with MRI images already acquired for clinical purposes and anonymized so that there is no possibility of direct or indirect identification of the patients. No additional information requiring new consent was collected. The study was conducted using exclusively radiographic images already acquired according to the traditional protocols of our institution.

## HUMAN AND ANIMAL RIGHTS

All human research procedures followed were in accordance with the ethical standards of the committee responsible for human experimentation (institutional and national), and with the Helsinki Declaration of 1975, as revised in 2013.

## CONSENT FOR PUBLICATION

Informed consent to MRI examination was obtained from all participants.

## STANDARDS OF REPORTING

STROBE guidelines were followed.

## AVAILABILITY OF DATA AND MATERIALS

The data and supportive information are available within the article.

## CONFLICT OF INTEREST

The authors declare no conflict of interest, financial or otherwise.

## ACKNOWLEDGEMENTS

Declared none.

## SUPPLEMENTARY MATERIALS

Supplementary material is available on the Publisher's website.

## REFERENCES

- [1] Patel AP, Fisher JL, Nichols E, *et al.* Global, regional, and national burden of brain and other CNS cancer, 1990–2016: A systematic analysis for the global burden of disease Study 2016. *Lancet Neurol* 2019; 18(4): 376–93.  
[http://dx.doi.org/10.1016/S1474-4422\(18\)30468-X](http://dx.doi.org/10.1016/S1474-4422(18)30468-X) PMID: 30797715
- [2] Nayak L, Lee EQ, Wen PY. Epidemiology of brain metastases. *Curr Oncol Rep* 2012; 14(1): 48–54.  
<http://dx.doi.org/10.1007/s11912-011-0203-y> PMID: 22012633
- [3] Ostrom Q T, Patil N, Cioffi G, Waite K, Kruchko C, Barnholtz-Sloan J S. Cbtrus statistical report: Primary brain and other central nervous system tumors diagnosed in the United States in 2013–2017. *Neuro Oncol* 2020; 22(12 Suppl 2): iv1–iv96.  
<http://dx.doi.org/10.1093/neuonc/noaa200> PMID: 33123732
- [4] Sawlani V, Patel MD, Davies N, *et al.* Multiparametric MRI: Practical approach and pictorial review of a useful tool in the evaluation of brain tumours and tumour-like lesions. *Insights Imaging* 2020; 11(1): 84.  
<http://dx.doi.org/10.1186/s13244-020-00888-1> PMID: 32681296
- [5] Martucci M. Magnetic resonance imaging of primary adult brain tumors: State of the art and future perspectives. *Biomedicines* 2023; 11(2): 364.  
<http://dx.doi.org/10.3390/biomedicines11020364> PMID: 36830900
- [6] Alhussen A, Anul Haq M, Ahmad Khan A, Mahendran RK, Kadry S. XAI-RACapsNet: Relevance aware capsule network-based breast cancer detection using mammography images via explainability O-net ROI segmentation. *Expert Syst Appl* 2025; 261: 125461.  
<http://dx.doi.org/10.1016/j.eswa.2024.125461>
- [7] Kujur A, Raza Z, Khan AA, Wechtaisong C. Data complexity based evaluation of the model dependence of brain MRI images for classification of brain tumor and Alzheimer's disease. *IEEE Access* 2022; 10: 112117–33.  
<http://dx.doi.org/10.1109/ACCESS.2022.3216393>
- [8] Jolliffe I T, Cadima J. Principal component analysis: A review and recent developments. *Philos Trans A Math Phys Eng Sci* 2016; 374(2065): 20150202.  
<http://dx.doi.org/10.1098/rsta.2015.0202> PMID: 26953178
- [9] Abdalla SA, Mustafa ZA, Abraham BA. Brain tumor classification using principal component analysis and artificial neural network. *J Clin Eng* 2019; 44(2): 70–5.  
<http://dx.doi.org/10.1097/JCE.0000000000000333>
- [10] Akbari H, Kazerooni AF, Ware JB, *et al.* Quantification of tumor microenvironment acidity in glioblastoma using principal component analysis of dynamic susceptibility contrast enhanced MR imaging. *Sci Rep* 2021; 11(1): 15011.  
<http://dx.doi.org/10.1038/s41598-021-94560-3> PMID: 34294864
- [11] Tandel G S. A review on a deep learning perspective in brain cancer classification. *Cancers* 2019; 11(1): 111.  
<http://dx.doi.org/10.3390/cancers11010111> PMID: 30669406
- [12] Lotan E, Jain R, Razavian N, Fatterpekar G M, Lui Y W. State of the art: Machine learning applications in glioma imaging. *AJR Am J Roentgenol* 2019; 212(1): 26–37.  
<http://dx.doi.org/10.2214/AJR.18.20218> PMID: 30332296
- [13] Tang D, Chen M, Huang X, *et al.* SRplot: A free online platform for data visualization and graphing. *PLoS One* 2023; 18(11):

0294236.  
<http://dx.doi.org/10.1371/journal.pone.0294236> PMID: 37943830
- [14] von Reppert M. Image-based search in radiology: Identification of brain tumor subtypes within databases using MRI-based radiomic features. *AJNR Am J Neuroradiol* 2025; ajnr.A8805.  
<http://dx.doi.org/10.3174/ajnr.A8805>
- [15] Tampu IE, Bianchessi T, Blystad I, *et al.* Pediatric brain tumor classification using deep learning on MR images with age fusion. *Neurooncol Adv* 2025; 7(1): vdae205.  
<http://dx.doi.org/10.1093/oaajnl/vdae205> PMID: 39777258
- [16] Ye J, Zhao Z, Ghafourian E, Tajally A, Alkhazaleh HA, Lee S. Optimizing the topology of convolutional neural network (CNN) and artificial neural network (ANN) for brain tumor diagnosis (BTD) through MRIs. *Heliyon* 2024; 10(16): 35083.  
<http://dx.doi.org/10.1016/j.heliyon.2024.e35083> PMID: 39687857
- [17] Mir M, Madhi ZS, Hamid AbdulHussein A, *et al.* Detection and isolation of brain tumors in cancer patients using neural network techniques in MRI images. *Sci Rep* 2024; 14(1): 23341.  
<http://dx.doi.org/10.1038/s41598-024-68567-5> PMID: 39375429
- [18] Gaikwad SB, Joshi MS. Brain tumor classification using principal component analysis and probabilistic neural network. *Int J Comput Appl* 2015; 120(3): 5-9.  
<http://dx.doi.org/10.5120/21205-3885>
- [19] Alhusseini AKH, Changizi DV. The evaluation of integrated perfusion - Weighted imaging diffusion and magnetic resonance spectroscopy methods accuracy for brain neoplasms diagnosis compared to pathology findings. *Int J Innov Res Med Sci* 2024; 9(01): 1-11.  
<http://dx.doi.org/10.23958/ijirms/vol09-i01/1754>
- [20] Romano A. Diffusion weighted imaging in neuro-oncology: Diagnosis, post-treatment changes, and advanced sequences-an updated review. *Cancers* 2023; 15(3): 618.  
<http://dx.doi.org/10.3390/cancers15030618> PMID: 36765575
- [21] Kitis O, Altay H, Calli C, Yuntun N, Akalin T, Yurtseven T. Minimum apparent diffusion coefficients in the evaluation of brain tumors. *Eur J Radiol* 2005; 55(3): 393-400.  
<http://dx.doi.org/10.1016/j.ejrad.2005.02.004> PMID: 16129247
- [22] Lee SC, Moon W-J, Choi JW, *et al.* Differentiation between primary central nervous system lymphoma and glioblastoma: Added value of quantitative analysis of CT attenuation and apparent diffusion coefficient. *J Korean Soc Magn Reson Med* 2012; 16(3): 226.  
<http://dx.doi.org/10.13104/jksmrm.2012.16.3.226>
- [23] Jung BY, Lee EJ, Bae JM, Choi YJ, Lee EK, Kim DB. Differentiation between glioblastoma and solitary metastasis: Morphologic assessment by conventional brain mr imaging and diffusion-weighted imaging. *Investig Magn Reson Imaging* 2021; 25(1): 23.  
<http://dx.doi.org/10.13104/imri.2021.25.1.23>
- [24] Barajas RF Jr, Hodgson JG, Chang JS, *et al.* Glioblastoma multiforme regional genetic and cellular expression patterns: Influence on anatomic and physiologic MR imaging. *Radiology* 2010; 254(2): 564-76.  
<http://dx.doi.org/10.1148/radiol.09090663> PMID: 20093527
- [25] Doskaliyev A, Yamasaki F, Ohtaki M, *et al.* Lymphomas and glioblastomas: Differences in the apparent diffusion coefficient evaluated with high b-value diffusion-weighted magnetic resonance imaging at 3 T. *Eur J Radiol* 2012; 81(2): 339-44.  
<http://dx.doi.org/10.1016/j.ejrad.2010.11.005> PMID: 21129872
- [26] Ellingson BM, Malkin MG, Rand SD, *et al.* Validation of functional diffusion maps (fDMs) as a biomarker for human glioma cellularity. *J Magn Reson Imaging* 2010; 31(3): 538-48.  
<http://dx.doi.org/10.1002/jmri.22068> PMID: 20187195
- [27] Hayashida Y, Hirai T, Morishita S, *et al.* Diffusion-weighted imaging of metastatic brain tumors: Comparison with histologic type and tumor cellularity. *AJNR Am J Neuroradiol* 2006; 27(7): 1419-25.  
 PMID: 16908550
- [28] Su Y, Wang J, Guo J, *et al.* Bi-exponential diffusion-weighted imaging for differentiating high-grade gliomas from solitary brain metastases: A VOI-based histogram analysis. *Sci Rep* 2024; 14(1): 31909.  
<http://dx.doi.org/10.1038/s41598-024-83452-x> PMID: 39738411
- [29] Jenkinson MD, Du Plessis DG, Walker C, Smith TS. Advanced MRI in the management of adult gliomas. *Br J Neurosurg* 2007; 21(6): 550-61.  
<http://dx.doi.org/10.1080/02688690701642020> PMID: 18071982
- [30] Sadeghi N, Salmon I, Tang BNT, *et al.* Correlation between dynamic susceptibility contrast perfusion MRI and methionine metabolism in brain gliomas: Preliminary results. *J Magn Reson Imaging* 2006; 24(5): 989-94.  
<http://dx.doi.org/10.1002/jmri.20757> PMID: 17031832
- [31] Higano S, Yun X, Kumabe T, *et al.* Malignant astrocytic tumors: Clinical importance of apparent diffusion coefficient in prediction of grade and prognosis. *Radiology* 2006; 241(3): 839-46.  
<http://dx.doi.org/10.1148/radiol.2413051276> PMID: 17032910
- [32] Tozer DJ, Jäger HR, Danchavijitr N, *et al.* Apparent diffusion coefficient histograms may predict low-grade glioma subtype. *NMR Biomed* 2007; 20(1): 49-57.  
<http://dx.doi.org/10.1002/nbm.1091> PMID: 16986106
- [33] Schoh S, Meyer J, Gawlitza M, *et al.* Diffusion-weighted MRI reflects proliferative activity in primary CNS lymphoma. *PLoS One* 2016; 11(8): 0161386.  
<http://dx.doi.org/10.1371/journal.pone.0161386> PMID: 27571268
- [34] Shim WH, Kim HS, Choi CG, Kim SJ. Comparison of apparent diffusion coefficient and intravoxel incoherent motion for differentiating among glioblastoma, metastasis, and lymphoma focusing on diffusion-related parameter. *PLoS One* 2015; 10(7): 0134761.  
<http://dx.doi.org/10.1371/journal.pone.0134761> PMID: 26225937
- [35] Capasso R, Negro A, Russo C, *et al.* Conventional and advanced MRI techniques in the evaluation of primary CNS Lymphoma. *Semin Ultrasound CT MR* 2023; 44(3): 126-35.  
<http://dx.doi.org/10.1053/j.sult.2023.02.003> PMID: 37245879
- [36] Lee EJ, terBrugge K, Mikulis D, *et al.* Diagnostic value of peritumoral minimum apparent diffusion coefficient for differentiation of glioblastoma multiforme from solitary metastatic lesions. *AJR Am J Roentgenol* 2011; 196(1): 71-6.  
<http://dx.doi.org/10.2214/AJR.10.4752> PMID: 21178049
- [37] Hassannejad E, Mohammadifard M, Payandeh A, *et al.* Correlation of ADC values of adult brain tumors with the diagnosis and pathological grade: A cross-sectional multicenter study. *Health Sci Rep* 2024; 7(6): 2110.  
<http://dx.doi.org/10.1002/hsr.2.2110> PMID: 38841116
- [38] Villanueva-Meyer JE, Mabray MC, Cha S. Current clinical brain tumor imaging. *Neurosurgery* 2017; 81(3): 397-415.  
<http://dx.doi.org/10.1093/neuros/nyx103> PMID: 28486641
- [39] Morabito R, Alafaci C, Pergolizzi S, *et al.* DCE and DSC perfusion MRI diagnostic accuracy in the follow-up of primary and metastatic intra-axial brain tumors treated by radiosurgery with cyberknife. *Radiat Oncol* 2019; 14(1): 65.  
<http://dx.doi.org/10.1186/s13014-019-1271-7> PMID: 30992043
- [40] Kim KJ, Park M, Joo B, Ahn SJ, Suh SH. Dynamic contrast-enhanced MRI and its applications in various central nervous system diseases. *Investig Magn Reson Imaging* 2022; 26(4): 256.  
<http://dx.doi.org/10.13104/imri.2022.26.4.256>
- [41] Kim DH, Choi SH, Ryoo I, *et al.* Differentiation of true recurrence from delayed radiation therapy-related changes in primary brain tumors using diffusion-weighted imaging, dynamic susceptibility contrast perfusion imaging, and susceptibility-weighted imaging. *J Korean Soc Magn Reson Med* 2014; 18(2): 120.  
<http://dx.doi.org/10.13104/jksmrm.2014.18.2.120>
- [42] Scola E, Desideri I, Bianchi A, *et al.* Assessment of brain tumors by magnetic resonance dynamic susceptibility contrast perfusion-weighted imaging and computed tomography perfusion: A comparison study. *Radiol Med* 2022; 127(6): 664-72.  
<http://dx.doi.org/10.1007/s11547-022-01470-z> PMID: 35441970
- [43] Kim YE, Choi SH, Lee ST, *et al.* Differentiation between glioblastoma and primary central nervous system lymphoma using dynamic susceptibility contrast-enhanced perfusion MR imaging: Comparison study of the manual versus semiautomatic

- segmentation method. *Investig Magn Reson Imaging* 2017; 21(1): 9.  
<http://dx.doi.org/10.13104/imri.2017.21.1.9>
- [44] Tietze A, Mouridsen K, Lassen-Ramshad Y, Østergaard L. Perfusion MRI derived indices of microvascular shunting and flow control correlate with tumor grade and outcome in patients with cerebral glioma. *PLoS One* 2015; 10(4): 0123044.  
<http://dx.doi.org/10.1371/journal.pone.0123044> PMID: 25875182
- [45] Kanli G. Quantitative pre-clinical imaging of hypoxia and vascularity using MRI and PET. *Methods Cell Biol* 2025; 289-328.  
<http://dx.doi.org/10.1016/bs.mcb.2024.10.016>
- [46] Horská A, Barker P B. Imaging of brain tumors: MR spectroscopy and metabolic imaging. *Neuroimaging Clin N Am* 2010; 20(3): 293-310.  
<http://dx.doi.org/10.1016/j.nic.2010.04.003> PMID: 20708548
- [47] Housni A, Boujraf S, Alami B, Benzagmout M, Maaroufi M. Assessment of primary brain lymphoma using multimodal magnetic resonance imaging and proton magnetic resonance spectroscopy. *Asian J Neurosurg* 2018; 13(4): 1205-8.  
[http://dx.doi.org/10.4103/ajns.AJNS\\_137\\_17](http://dx.doi.org/10.4103/ajns.AJNS_137_17) PMID: 30459895
- [48] Taillibert S, Guillemin R, Menuet C, *et al.* Brain lymphoma: Usefulness of the magnetic resonance spectroscopy. *J Neurooncol* 2008; 86(2): 225-9.  
<http://dx.doi.org/10.1007/s11060-007-9468-2> PMID: 17786533
- [49] Lu SS, Kim SJ, Kim HS, *et al.* Utility of proton MR spectroscopy for differentiating typical and atypical primary central nervous system lymphomas from tumefactive demyelinating lesions. *AJNR Am J Neuroradiol* 2014; 35(2): 270-7.  
<http://dx.doi.org/10.3174/ajnr.A3677> PMID: 23928144
- [50] Yamasaki F, Takayasu T, Nosaka R, *et al.* Magnetic resonance spectroscopy detection of high lipid levels in intraaxial tumors without central necrosis: A characteristic of malignant lymphoma. *J Neurosurg* 2015; 122(6): 1370-9.  
<http://dx.doi.org/10.3171/2014.9.JNS14106> PMID: 25748300
- [51] Arévalo-Sáenz A, Rodríguez-Boto Amago G, Pedrosa Sánchez M. High-grade glioma and solitary metastasis: Differentiation by spectroscopy and advanced magnetic resonance techniques. *Egypt J Neurosurg* 2022; 37(1): 34.  
<http://dx.doi.org/10.1186/s41984-022-00172-y>
- [52] Fordham AJ, Hachert CC, Patel N, *et al.* Differentiating glioblastomas from solitary brain metastases: An update on the current literature of advanced imaging modalities. *Cancers* 2021; 13(12): 2960.  
<http://dx.doi.org/10.3390/cancers13122960> PMID: 34199151

**DISCLAIMER:** The above article has been published, as is, ahead-of-print, to provide early visibility but is not the final version. Major publication processes like copyediting, proofing, typesetting and further review are still to be done and may lead to changes in the final published version, if it is eventually published. All legal disclaimers that apply to the final published article also apply to this ahead-of-print version.